Int. J. Nonlinear Anal. Appl. 13 (2022) 2, 3281–3289
ISSN: 2008-6822 (electronic)
http://dx.doi.org/10.22075/ijnaa.2022.6847

Classification of lung cancer histology using CT images based on convolutional neural network-CNN

Abd Al-Baset Rashed Saabia[a,*], Raghad Majeed Azawi[b], Rasha Amer Kadhim[c]

[a]Ministry of Education, The General Directorate for Education of Diyala, Iraq
[b]Computer of Science, College of Medicine, Diyala University, Diyala, Iraq
[c]College of Agriculture, University of Diyala, Diyala, Iraq

(Communicated by Madjid Eshaghi Gordji)

Abstract

In the field of medical imaging, interest in deep learning as a talented new discipline and a key component is growing rapidly. In lung cancer, the histology of tumours is a key predictor of therapy response and outcome. The most accurate way to classify histologies is through a pathologist's examination of tissue samples. Early tumour detection and therapy are essential for patients' recovery. For the purpose of identifying illness signs and risk stratification, recent developments in machine learning, medical image processing, and the use of radiologic data are highlighted. Regarding lung cancer and its various subtypes, it is error-prone and time-consuming to identify and differentiate. Convolutional Neural Networks can more accurately and quickly diagnose different types of lung cancer, which is essential for choosing the best treatment plan and patient survival rate. This research is concerned with both malignant (tumour) and benign tissue cell carcinomas. A training accuracy of 98.60 percent is obtained for the classification system of the suggested system, which is superior to that of both classic neural networks and the CNN model.

Keywords: Deep Learning, Tumors, Classification, Convolutional Neural Network, Accuracy
2020 MSC: 68T07

1 Introduction

Early detection of tumour (cancer) is the greatest promising approach to enhance a patient's casual for survival. This particular type of lung cancer is a common malignancy in both men and women, accounting for about (25 percent) of all cancer fatalities [9]. About (80%) of death is from smoking and the major reason for lung tumour. While in non-smokers people can be caused via second-hand smoke, exposure toward radon, air litter or other elements like workstation exposures to asbestos, sure other chemicals lung tumours some people who don't smoke or diesel exhaust [7].

Many experiments similar to imaging groups (CT scan, X-ray), sputum cytology and tissue collection or biopsy are recommended in order to look for malignant cells and rule out other potential illnesses. To determine the diagnosis and describe the various types and subtypes of lung illnesses, skilled pathologists must evaluate microscopic histopathology

*Corresponding author
Email addresses: abdalbast.rsheed@gmail.com (Abd Al-Baset Rashed Saabia), mraghad699@gmail.com (Raghad Majeed Azawi), rashakadhim@uodiyala.edu.iq (Rasha Amer Kadhim)

Received: June 2022 *Accepted:* August 2022

slides while performing the biopsy [5]. The chief histological kinds of Lang tumour "include adenocarcinoma (ADC), and "squamous cell carcinoma" (SCC), which originate from the small and large airway epithelia, respectively. The misdiagnosis of cancer classifications, which results in improper treatment and could result in patient deaths, is a significant development. Machine learning (ML) is a branch of artificial intelligence (AI) that exposes machines to collections of data and enables them to learn certain tasks via experience without explicit programming [4].

In this work, an intelligent scheme was built to detect lung tumour early and classify them with high accuracy to help doctors and patients not to exacerbate and control the disease before it was too late. As a result, human life is saved. This research work presents lung cancer classification using [4] CT images. The model was able to succeed and achieve High and advanced of training and support accuracy. To evaluate the model's performance, recall, f1 scores, and precision were calculated. Additionally, a confusion matrix plot was made. This study's advantage is that it will take less time and effort for medical professionals to diagnose patients accurately and quickly in order to prevent further disease exacerbations.

2 Literature Review

In 2021, Using a dataset of (311) early-stage neural networks, Tafadzwa L. et al. [6] suggested a method for training and evaluating convolutional neural networks (CNNs) (NSCLC patients). The CNN's AUC for predicting tumor histology was 71% ($p = 0.018$). On CNN-derived quantitative radionics characteristics, it was discovered that applying machine learning classifiers like (KNN) and (SVM) produced equivalent performance in discrimination with an AUC of up to 71% ($p = 0.017$). The most effective probabilistic classifier was Top CNN.

In 2020, Asuntha A. et al. [1] specified a way to identify and classify malignant tissues by utilizing a DL style. As the input picture, CT images were used with a LIDC-isolated dataset, and Histogram Equalization (HE) was applied to enhance the difference values. In pre-processing stage was used the "adaptive Bilateral filtering technique" for de-noise the CT images. In the segmentation, the stage was used "artificial Bee Colony segmentation algorithm" for extract the ROI and segment image. In Next stage was to extract 180 features by utilizing Local-Binary Pattern, wavelet methods, the best relevant features were then selected using fuzzy particle swarm optimization (FPSO), which was then used to reduce the density for the CNN average, which is then used to classify the extracts as "benign or malignant." The proposed typical's average accuracy rate is 95.62%, and its specificity and sensitivity are 95.89%, and 96.23%, respectively.

In 2019, Tekade R. et al. [19] offered a method utilizing two types, the first for image segmentation and the second for determining the amount of malignancy. CNN is used in the stage determination process with two FEs for categorization. In this manner, ReLU is the starting function for sub pooling, the classifier used to do classification prior to presenting the malignant-level information is called soft-max. This method employs U-Net to segment and further predict levels of malignancy, and it has a 95.66% accuracy rate, a loss of (0.09), a dice number of (90%) and an estimated log loss of (38%).

In 2018, Sasikala S. et al. [17] submitted CNN-based methodology, experiments were performed on 472-patients. These datasets are classified for either [T1, T2 or T3, T4] utilizing the CNN algorithm. The scheme was advanced utilizing 2 networks feature extractor and classifier. FE was utilized into relevant-feature that is to be extracted and a classifier algorithm was based on classifying-patch. The results of the scheme are 69% for accuracy rate, 69% for testing, and 87% for training sets.

In 2017, to minimize overfitting, gathered images were enhanced using rotation, flipping, and filtering after Tetsuya T. et al. [20] Presented his DCNN classifier in microscopic images that had a resolution of (256 x 256) pixels were first gathered and resampled. The system that was being created was used to determine the likelihood of three different cancer kinds, and its classification accuracy was evaluated using threefold cross-validation. Comparable to the accuracy of cytotechnologists and pathologists, roughly (71%) of the pictures were properly categorized, according to the results. Consequently, the emerging method is appropriate for classifying lung tumors from microscopic pictures.

3 Proposed System

Our Proposed System followed the data acquisitions phase, preprocessing phase, segmentation phase, and classification phase (training and testing). The proposed approach is based on the CNN design for the classification of the image. The steps of system intricate are as follows:

Step1: Acquisition for CT lung images.

Step2: Preprocessing by utilizing Gabor Filter.

Step3: Image segmentation by utilizing Marker Controlled Watershed.

Step4: Feature extraction by utilizing FDCT and GLCM.

Step5: Classification by utilizing the CNN algorithm. As shown in figure 1 and described in the below sections.

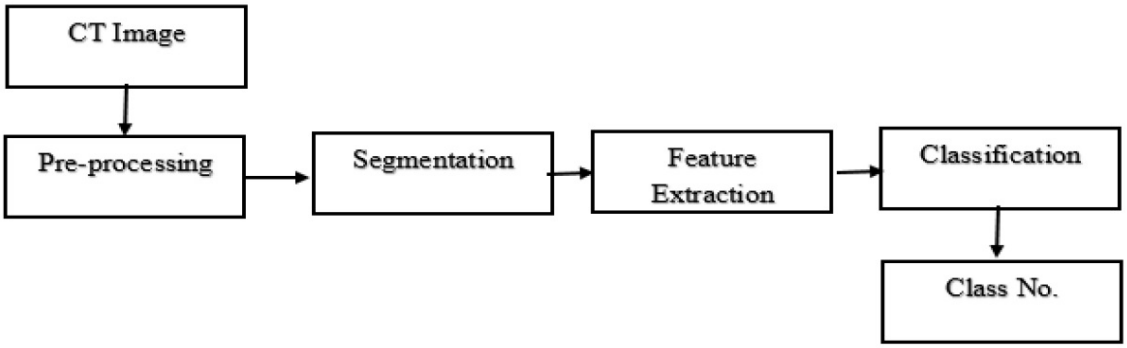

Figure 1: Block Diagram of Proposed System

3.1 Data Acquisition

The histopathology images were obtained from the LC-25000 Lung histopathological CT image dataset from Al-Yarmouk Teaching Hospital. For our work, 300 histopathological photos from each of the three classifications of lung cancer and tumors—"benign tissue, adenocarcinoma, and squamous carcinoma cells"—were taken into consideration.

3.2 Pre-processing

Pre-processing is a word used in the public referring to activities where the input and output images are both strong images at the Lowest-Level of Concept. Usually, a matrix of image function values shows how strong an image is. These recognizable images have the same high quality as the original data from the sensor [21]. Although geometry transformations of images (such as scaling, translation, and rotation) are categorized among preprocessing approaches here as similar technique is employed, the goal from this step is a development and improvement of data image that prevents changes from occurring or enhances certain image features necessary for subsequent processing. Pre-processing of photographs is necessary to advance contrast, clarity, and isolate contextual noise. As a result, several techniques, including smoothing and augmentation, are used to obtain photos in the required format [10].

3.2.1 Enhancement

The enhancement process is utilized into developing and enhance the interpretability or opinion within the information of input images aimed at human observers, or into make available well input for other mechanical image processing methods. There are two basic categories of image enhancement: (frequency domain and spatial domain). Here, Gabor filter is used to determine enhancement since it has a good result rate when compared to fast Fourier and automatic enhancement [14].

3.2.2 Gabor filter

It's a linear filter used for texture analysis, which means that it basically determines whether a particular frequency is present in the image in precise directions inside a confined region around the analysis point or region. Although there are no empirical proofs and no practical justification for the claim, many vision engineers today insist that the frequency and orientation of Gabor filter drawings are the same as those of the human visual system [15]. Its impulse reaction or response is definite via a sinusoidal wave (an even wave for 2-D Gabor filters) multiplied through a Gaussian function as shown in figure 2: (a) Lung input image and (b) after applying the Gabor filter output image. . Because of the multiplication-convolution stuff, the Fourier transform for a Gabor filter's intuitive response is the convolution of the Fourier transform for the harmonic function (sinusoidal function) and the Fourier transform of the Gaussian function (convolution theorem) [16].

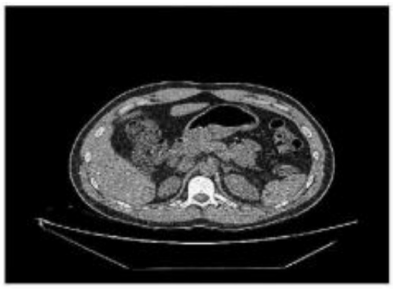

(a): Lung input image.

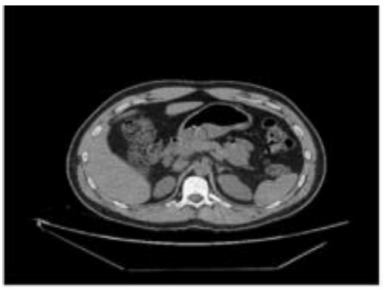

(b): Gabor filter output image.

Figure 2: Pre-processing Enhancement Output

3.3 Image Segmentation

It's a method that split an image into different areas, which are homogeneous in some characteristics. It is the primary step and very important in various image processing uses and applications like Pattern recognition and image analysis. Image analysis includes object description and representation and feature measurement. In image segmentation, numerous existing methods are utilized [12].

3.3.1 Watershed Segmentation

These watershed-based systems utilize the concept or idea of topological interpretation. In this method the intensity signifies the basins having dump (hole) in their minima from where the waterfalls (spills). When water ranges the border and edges of the basin the adjacent basins will be merged [8]. And the pixels having additional gradients are characterized as boundaries that are incessant. Then watershed segmentation to discrete moving objects Gray-scale image (Binary image Enhancement Image from the pre-processing stage) read in images. Then watershed transform is repeatedly functional of problem in this. And the watershed transforms discovery in an image is "Watershed troughs" and "watershed ridge lines" can be seen where pixels that are light are high and pixels that are dark are low [15].

3.3.2 Marker Controlled Watershed Segmentation

It is a robust and flexible scheme for the segmentation of objects with closed outlines, where the borders are expressed (spoken) as ridges. The marker image utilized in the watershed segmentation process is a binary image containing either single-marker points or larger-marker regions and where each related marker is sited inside an object of interest. The block diagram of watershed segmentation is shown in figure 3. The marker is created automatically positioned and thereby avoiding the problem of over-segmentation, and manual marking speedy detection in both (edges and regions) [18]. Figure (4 (a,b)) illustrations the results of the steps of the segmentation process.

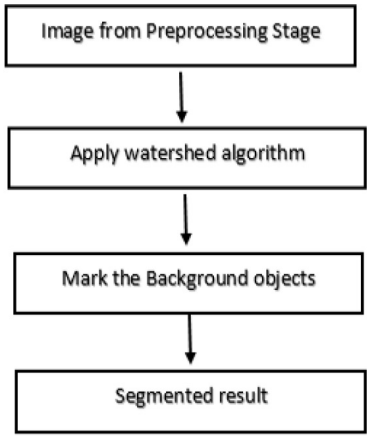

Figure 3: Block diagram of watershed segmentation stage

(a) Patch Extraction (b) Object boundaries segmented image

Figure 4: The results of the steps of the segmentation process.

3.3.3 Curve let Transform

It's a single element in transforms utilized to Multi-Scale Geometric Analysis which tries toward overawed the restriction in customary DWTs. It is a multi-scale pyramid within several instructions and locations in apiece length measure, and needle-formed features on well scales [13]. Figure 5 explains the method of curve let transform.

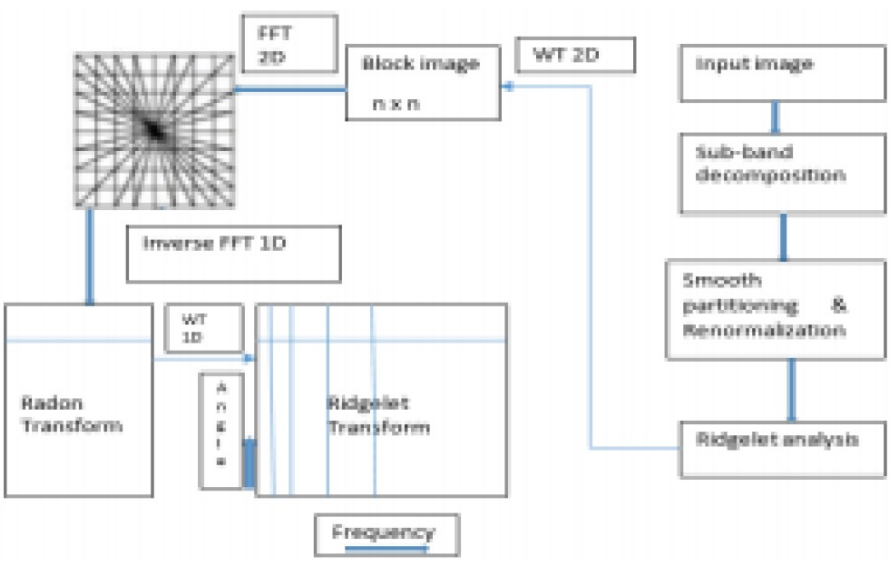

Figure 5: The Method of Curve let Transform.

There are two approaches utilized for finding the curve let coefficients are (USFFT) and packaging based on ways. Unequal sample the Fourier models in the image is done within US FFT, while wrapping created technique utilizes a sequence for transformation and wrap round way into getting the curve let coefficients. Although the results of combining the procedures are comparable, the wrapping-based process is efficient for computation. A wrapping-based method is used in the suggested work. Utilizing F FT techniques, the coefficients of the curve let are produced [3].

3.4 Feature Extraction based GLCM

It is a second order-statistical technique in features extraction processes that calculation for textual features and computes the GLCM. In the collection and determining one nation for distinct features as per shape, texture, color, and contrast, the accuracy for the medicinal analysis-system can be improved effectively [8]. In general, the variance and mean in the intensity for the voxelsareely the 1st-order features. Additionally, the link between the voxels in the account is won in order to take into account the second-order features [2]. The frequency of occurrence from gray levels for different directions is detailed using GLCM. Typically, the angle of dissimilarity is $\emptyset = 0°$. The α significant features, including "energy (ASM), contrast, homogeneity (IDE), correlation, and entropy," that Haralick proposed for 14 characteristics are calculated for feature extraction [2].

$$The\ homog.(IDE) = \sum_i \sum_j \frac{1}{1+(i-j)^2} p(i,j) \tag{3.1}$$

$$Energy(ASM) = \sum_i \sum_j p(i,j) \tag{3.2}$$

$$Correlation = \frac{\sum_i \sum_{j(i,j)} p(i,j)\mu x\ \mu y}{\sigma x\ \sigma y} \tag{3.3}$$

where $\sigma x, \sigma y, \mu x$ and μy are the standard deviations and means of p_x and p_y.

$$\mu x = \sum_i \sum_j p(i,j) \tag{3.4}$$

$$\sigma x = \sum_a (a-\mu x)^2 \sum_b p(a-b) \tag{3.5}$$

$$Entropy = \sum_i \sum_j p(i,j) \log_2 p(i,j) \tag{3.6}$$

$$Contrast = \sum_i \sum_j p(i,j) * (i-j)^2 \tag{3.7}$$

3.5 Classification

The CNN design is an entity that can be described mathematically. It is made up of several "feed-forward layers as per- convolution-layer and pooling-layer" delay spread across one or more completely linked layers. Convolution and pooling in the first two layers help extract features, which are then sketched into the final output and exchanged as 2D feature maps into 1D vectors to help categorize the dataset images. The CNN algorithm can be trained in the cut for image classification, or pre-trained CNN features can be purchased and employed, or supervised methods can be used to refine unsupervised CNN pre-training [13]. Each neuron in CNN is connected to every other neuron in the "Receptive Field" layer, which is the following layer. The receptive field, which is often a square, is the area or region in the CNN algorithm that is associated with one neuron in the following [11].

3.5.1 Convolution layer

It is crucial to the CNN algorithm's ability to build a stack of convolutional mathematical operations. Using "an optimizable feature extractor within the input image whose pixels are preserved in 2D array," the kernel is convolved [22], and the feature diagram is created. The kernel's size affects how deep the resulting feature-map is (typically 3×3 or 5×5). Figure 6 depicts a convolution process illustration.

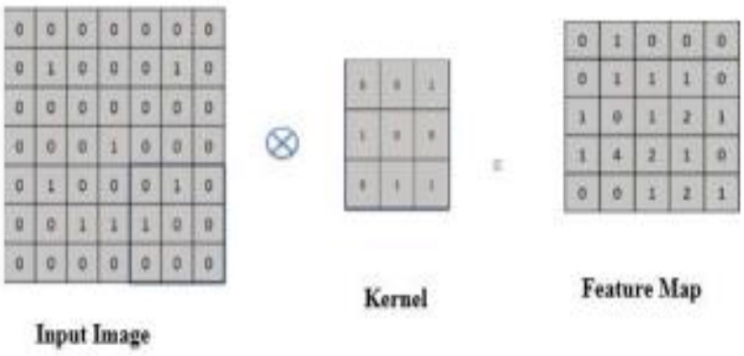

Figure 6: Convolution Process Example with 3×3 Kernel Size.

3.5.2 Pooling Layer or (subsampling)

After the convolutional layer that shrink's models, this layer is introduced, and its primary function is to shrink in-space measurement (dimension) for feature charts. The two advantages of using pooling layers for size reduction are fewer computational layers above the forthcoming levels and the ability to work alongside above suitable [13]. Average pooling is the most frequently used pooling procedure, and max poo ling is pronounced mathematically identically:

$$\alpha_j = \max_{(p,q)\in Rji} \alpha_{kqp} \tag{3.8}$$

$$\alpha_{kij} = \frac{1}{|Rij|}\sum(p,q) \in \alpha_{kpq} \tag{3.9}$$

where α_j is max poo ling and α_{kij} is Average poo ling.

The misperception matrix-plot was used to measure the performance of the industrialized CNN type or technique, and the recall, precision, f1-score, and metrics accuracy were also intended as per below:

$$Accuracy = \frac{(TP+TN)}{(TP+FP+FN+TN)} \tag{3.10}$$

$$Precision = \frac{TP}{(TP+FP)} \tag{3.11}$$

$$Recall = \frac{TP}{(TP+FN)} \tag{3.12}$$

$$F1-Score = \frac{2*(Recall*Precision)}{(Recall+Precision)} \tag{3.13}$$

Where the TN is true negative, FN is false negative, FP is false positive, and TP stands for true positive values for the representations' training and validation images. The training standard weights were retained in the /hd5-file design and were used for forecasting the future by stacking the weights in a conventional manner.

4 Result and Discussion

This system used 300 images of CT lung cancer for each category. The images were trained 150 times with 256×256 -pixel batch sizes and 211 epochs. In the end, the model had a training accuracy of 98.40% and a proof accuracy of 99.20% in the final time. For training and validation images, Figure 7(b) depicts the model loss vs. epoch, while 7(a) depicts the model accuracy. The precision, recall, and f-score for the several renthistopathological picture categories are displayed in Table 1. Finally, yet importantly, Figure 8 shows how CNN's activity works (ReLU, sigmoid and tan). CNN algorithm can discover delicate variances in images to expect phenotypes in future cases14. In these digital photos, we were able to build on previously acquired low-/mid-level characteristics by using pre-trained methods (e.g., texture, shadows, edges etc.). Given the magnitude of the partial size dataset, the high dimensionality of the features, and the relatively big schemes, T is decreasing the likelihood of over-fitting. Additionally, it made it possible for the simulations to more successfully interpret heterogeneous picture data, enabling a robustness to variances in regularly obtained clinical data.

Table 1: F1-Score, Recall, and Precision of System for Different Categories

Category	Precision	Recall	F1-Score
Benign tissue	1	1	1
Adenocarcinoma	0.96	0.98	0.97
Squamous Cell Carcinoma	0.98	0.96	0.97

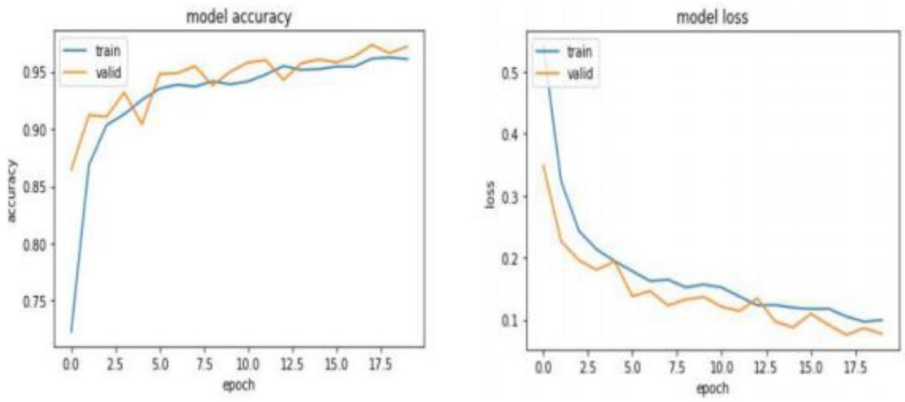

(a) (b)

Figure 7: (a) a) the plot of Model Accuracy vs. Training and Validation Epoch. (b) the plot of Model Loss vs . Training and Validation Epochs.

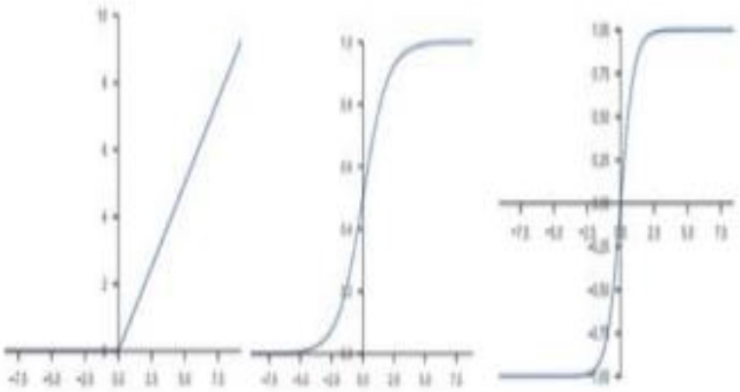

Figure 8: The CNN activity functions (ReLU, Sigmoid, and Tan).

5 Conclusion

In this study, CT images are used to classify lung cancer. Images of three distinct categories—benign tumors, squamous cell carcinoma, and adenocarcinoma—were classified using a CNN. The model was successful and was able to reach training and support accuracy of 98.40%. To evaluate the model's performance, a confusion matrix plot was made after precision, f1-scores, and recall were computed. The benefit of this study is to reduce the effort on doctors and give a correct and rapid diagnosis to protect patients from further exacerbation of the disease, so we recommend the establishment of a system to detect lung diseases and classify them and to develop a new method by using Transform Multi Layers Wavelet and Probabilistic Neural Network (PNN) algorithm.

References

[1] A. Asuntha and A. Srinivasan, *Deep learning for lung cancer detection and classification*, Multimedia Tools Appl. **79** (2020), no. 11, 7731–7762.

[2] R.M. Azawi, D.A. Abdulah, J.M. Abbas and I.T. Ibrahim, *Brain tumors classification by using gray level co-occurrence matrix, genetic algorithm and probabilistic neural network*, Diyala J. Med. **14** (2018), no. 2.

[3] R.M. Azawi, D.A. Abdulah, J.M. Abbas and I.T. Ibrahim, *A hybrid approach for classification of MRI brain tumors using genetic algorithm, K-nearest neighbor and probabilistic neural network*, Int. J. Comput. Sci. Inf. Secur. **16** (2018), no. 5.

[4] D. Bazazeh and R. Shubair, *Comparative study of machine learning algorithms for breast cancer detection and diagnosis*, Int. Conf. Electronic Devices Syst. Appl., 2016, pp. 1–4.

[5] K. Bijaya and C. Himal, *Lung cancer detection using convolutional neural network histopathological images*, Int. J. Comput. Trends Techn. **68** (2020), no. 10.

[6] T.L. Chaunzwa, A. Hosny, Y. Xu, A. Shafer, N.Diao, M. Lanuti, D.C. Christiani, R.H. Mak and H.J. Aerts, *Deep learning classification of lung cancer histology using CT images*, Sci. Rep. **11** (2021), no. 1–12.

[7] M.R. Davidson, A.F. Gazdar and B.E. Clarke, *The pivotal role of pathology in the management of lung cancer*, J. Thoracic Disease **5** (2013), no. Suppl 5, p. S463.

[8] M. Heba, A. Sayed, M. Sayed and M. Abdel Badeeh, *Classification using deep learning neural networks for brain tumors*, Future Comput. Inf. J. **3** (2018), no. 1, 68–71.

[9] T. Huang, *Distinguishing lung adenocarcinoma from lung squamous cell carcinoma by two hypo methylated and three hyper methylated genes: A meta-analysis*, PLoS ONE **11** (2016).

[10] T. Ibrahim, M. Sabah, Z. Anmar and Al-M Emad, *The evaluation of calcium score validity in the diagnosis of patients with coronary artery disease by using CT angiography*, Diyala J. Med. **9** (2015), no. 1.

[11] P.M. Krishnammal and S.S. Raja, *Convolutional neural network-based image classification and detection of abnormalities in MRI brain images*, Int. Conf. Commun. Signal Process., 2019, pp. 548–553.

[12] X. Li, S. Luo, Q. Hu, J. Li, D. Wang and F. Chion, *Automatic lung field segmentation in X-ray radiographs using statistical shape and appearance models*, J. Med. Image Health Inf. **6** (2016), 338–348.

[13] J. Liu and L. Guo, *A new brain MRI image segmentation strategy based on wavelet transform and K-means clustering*, IEEE Int. Conf. Signal Process. Commun. Comput., 2015, pp. 1–4.

[14] Z. Majd, A. Pim and D. Bob, *Automatic calcium scoring in low-dose chest CT using deep neural networks with dilated convolutions Nikolas Lessmann, Bram van Ginneken*, Member IEEE Trans. Med. Imag. **37** (2018), no. 2, 615–625.

[15] R. Prajwal, A. Nishal and S. Raghuram, *Convolutional neural networks for lung cancer screening in computed tomography (CT) scans*, 2nd Int. Conf. Contemp. Comput. Inf., IEEE, 2016, pp. 489–493.

[16] A. Rasha and K. Muntadher, *A real-time American sign language recognition system using convolutional neural network for real datasets*, TEM J. **9** (2020), no. 3.

[17] S. Sasikala, M. Bharathi and B.R. Sowmiya, *Lung cancer detection and classification using deep CNN*, Int. J. Innov. Tech. Explor. Eng. **8** (2018), no. 25, 259–262.

[18] H. Shin, H.R. Roth, M. Gao, L. Lu, Z. Xu, I. Nogues, J. Yao, D. Mollura and R. M. Summers *Deep convolutional neural networks for computer-aided detection: CNN architectures, dataset characteristics and transfer learning*, IEEE Trans. Med. Imag.**35** (2016), no. 5, 1285–1298.

[19] R. Tekade and K. Rajeswari, *Lung cancer detection and classification using deep learning*, Int. Conf. Comput. Commun. Control Autom., 2019, pp. 1–5.

[20] A. Teramoto, T. Tsukamoto, Y. Kiriyama and H. Fujita, *Automated classification of lung cancer types from cytological images using deep convolutional neural networks*, BioMed Res. Int. **2017** (2017).

[21] J. Xu, X. Luo, G. Wang, H. Gilmore and A. Madabhu, *A deep convolutional neural network for segmenting and classifying epithelial and stromal regions in histopathological images*, Neurocomput. **191** (2016), 214–223.

[22] R. Yamashita, M. Nishio, R.K.G. Do and K. Togashi, *Convolutional neural network: An overview and application in radiology*, Insights Imag. **9** (2018), no. 4, 611–629.